AFRL-PR-WP-TP-2007-204

DIODE LASER DIAGNOSTICS OF HIGH SPEED FLOWS (POSTPRINT)

Skip Williams, Dominic Barone, Todd Barhorst, Kevin, Jackson, and K.-C. Lin

Propulsion Sciences Branch
Aerospace Propulsion Division

OCTOBER 2006

AIR FORCE RESEARCH LABORATORY
PROPULSION DIRECTORATE
WRIGHT-PATTERSON AIR FORCE BASE, OH 45433-7251
AIR FORCE MATERIEL COMMAND
UNITED STATES AIR FORCE

REPORT DOCUMENTATION PAGE

Form Approved
OMB No. 0704-0188

1. REPORT DATE *(DD-MM-YY)*	2. REPORT TYPE	3. DATES COVERED *(From - To)*
October 2006	Conference Paper Postprint	30 March 2006 – 10 September 2006

4. TITLE AND SUBTITLE
DIODE LASER DIAGNOSTICS OF HIGH SPEED FLOWS (POSTPRINT)

5a. CONTRACT NUMBER
In-house

5b. GRANT NUMBER

5c. PROGRAM ELEMENT NUMBER
61102F

6. AUTHOR(S)
Skip Williams, Dominic Barone, Todd Barhorst, Kevin, Jackson, and K.-C. Lin (AFRL/PRAS)
Pat Masterson, Qingchun Zhao, and Andrew D. Sappey (Zolo Technologies, Inc.)

5d. PROJECT NUMBER
2308

5e. TASK NUMBER
AI

5f. WORK UNIT NUMBER
2308AI01

7. PERFORMING ORGANIZATION NAME(S) AND ADDRESS(ES)

Propulsion Sciences Branch (AFRL/PRAS)
Aerospace Propulsion Division
Air Force Research Laboratory, Propulsion Directorate
Wright-Patterson Air Force Base, OH 45433-7251
Air Force Materiel Command, United States Air Force

Zolo Technologies, Inc.
4946 N 63rd Street
Boulder, CO 80301

8. PERFORMING ORGANIZATION REPORT NUMBER
AFRL-PR-WP-TP-2007-204

9. SPONSORING/MONITORING AGENCY NAME(S) AND ADDRESS(ES)
Air Force Research Laboratory
Propulsion Directorate
Wright-Patterson Air Force Base, OH 45433-7251
Air Force Materiel Command
United States Air Force

10. SPONSORING/MONITORING AGENCY ACRONYM(S)
AFRL/PRAS

11. SPONSORING/MONITORING AGENCY REPORT NUMBER(S)
AFRL-PR-WP-TP-2007-204

12. DISTRIBUTION/AVAILABILITY STATEMENT
Approved for public release; distribution unlimited.

13. SUPPLEMENTARY NOTES
Conference paper published in the Proceedings of the 14th AIAA/AHI International Space Planes and Hypersonic Systems and Technologies Conference.

PAO Case Number: AFRL/WS 06-2229, 02 Oct 2006.

14. ABSTRACT
This document contains the specific requirements and preliminary results for the Optical Mass Capture (OMC) experiment for the Fundamental RESearch Hypersonic Flight experimentation (FRESH Fx) program. The objective of this effort is to develop and demonstrate in flight a diode-laser-based measurement of engine air mass capture in the inlet or isolator of . a hypersonic vehicle over an altitude range of 60,000-90,000 ft with an average Mach number of 7.5 over this range. The concept involves the direct measurement of oxygen concentration via absorption spectroscopy, and gas velocity via the Doppler shift of laser light transiting the flowpath. The deduced density-velocity product in a known flow area yields the mass flow rate.

15. SUBJECT TERMS
DIODE LASER SPECTROSCOPY, SUPERSONIC COMBUSTION, MASS CAPTURE, FLIGHT DIAGNOSTICS

16. SECURITY CLASSIFICATION OF:			17. LIMITATION OF ABSTRACT:	18. NUMBER OF PAGES	19a. NAME OF RESPONSIBLE PERSON (Monitor)
a. REPORT	b. ABSTRACT	c. THIS PAGE			Dr. Skip Williams
Unclassified	Unclassified	Unclassified	SAR	22	19b. TELEPHONE NUMBER *(Include Area Code)* N/A

Standard Form 298 (Rev. 8-98)
Prescribed by ANSI Std. Z39-18

Diode Laser Diagnostics for High Speed Flows

Skip Williams[1], Dominic Barone[2], Todd Barhorst[2], Kevin Jackson[2] and K.-C. Lin[3]
Air Force Research Laboratory, Propulsion Directorate, 1950 Fifth Street, WPAFB, OH 45433

and

Pat Masterson[4], Qingchun Zhao[5], and Andrew D. Sappey[6]
Zolo Technologies, Inc., 4946 N 63rd Street, Boulder, CO 80301

Tunable diode laser absorption spectroscopy (TDLAS) using single mode diode lasers that are temperature stabilized and current tuned were used to measure the air velocity in the isolator section of a research scramjet flowpath. Tests were conducted in the Research Cell 18 direct connect wind tunnel facility at WPAFB. TDLAS was used to detect water and oxygen at concentrations of $2.2x10^{17}$ cm^{-3} and $1.8x10^{18}$ cm^{-3}, respectively, in the isolator operated at simulated flight Mach numbers of 3.5 and 4.0 and a dynamic pressure of 1000 psf. To achieve these simulated flight conditions, a natural gas fueled vitiator was used to elevate the air temperature, and a Mach-1.8 facility nozzle was installed to expand the flow. The velocity was determined at these conditions, and above and below, by varying the vitiator temperature in 100ºR increments from 798ºR to 1593ºR in order to provide calculated flow velocities from 600 m/s to 850 m/s based on isentropic equations. The TDLAS velocity data agree to within 22 m/s and 32 m/s (1 σ) for data obtained at 100 millisecond and 10 millisecond sampling intervals, respectively.

Nomenclature

c	=	speed of light
θ	=	crossing angle of laser beam with the flow direction
FL	=	focal length
NA	=	numerical aperture
Q	=	dynamic pressure in psf
u	=	bulk flow velocity
$\Delta\nu$	=	Doppler frequency shift
ν_o	=	line center frequency,

I. Introduction

The Propulsion Directorate of the Air Force Research Laboratory (AFRL/PR) at Wright-Patterson Air Force Base (WPAFB), among others, is developing in-situ combustion performance diagnostics using diode laser sensors for test applications where the determination of species concentration, temperature, and velocities in high speed flows are required. Generally, wall measurements (e.g. pressure, temperature, and heat flux) dominate the instrumentation suite routinely employed. If in-stream information (usually pitot pressure) is available, it is usually sparse and is generally available only at the inflow and outflow planes of the test article. Diode laser based techniques are practical in terms of weight, power, and optical access requirements and have the additional advantage of being able to provide in-stream information as well. One in-stream measurement of particular interest is the measurement of

[1] AIAA senior member, Corresponding Author, skip.williams@wpafb.af.mil
[2] AIAA member.
[3] Taitech, Inc., 1430 Oak Court, Suite 301, Beavercreek, OH 45430, Senior Member AIAA.
[4] Electro-Optic Engineer, Zolo Technologies, Inc., 4946 N 63rd Street, Boulder, CO 80301.
[5] Software Engineer, Zolo Technologies, Inc., 4946 N 63rd Street, Boulder, CO 80301.
[6] Chief Technology Officer, Zolo Technologies, Inc., 4946 N 63rd Street, Boulder, CO 80301.

mass flux defined as the product of air velocity and air density. The current standard for measuring mass flux in ground test facilities is through the use of total and static pressure probes and total temperature or thermocouple probes. This instrumentation requires the insertion of an instrumented, intrusive probe into the flowpath. Furthermore, the time response of this instrumentation is limited making the observations of transient conditions difficult to study. Diode laser-based approaches offer the ability to probe high speed flows non-intrusively and in real-time, as short as one millisecond for some applications.

This paper describes our efforts to develop tunable diode laser absorption spectroscopy (TDLAS) using single mode diode lasers that are temperature stabilized and current tuned to measure the mass flux in the isolator section of a research scramjet flowpath in real time (~ 10 ms). The test article is operated in a direct connect wind tunnel facility within Research Cell 18 at WPAFB. Molecular oxygen was detected and quantified by tuning a diode laser over selected transitions of the $b^1\Sigma_g^+ - X^3\Sigma_g^-$ (atmospheric) system at 760 nm. The measurements involve the direct measurement of oxygen concentration via absorption spectroscopy, and gas velocity via the Doppler shift of laser light transiting the flowpath. The details of our initial measurements and preliminary results are discussed below.

II. Facility

AFRL/PR owns and operates two direct-connect supersonic combustion facilities. Figure 1 shows a schematic of the Research Cell 18 testing article where the experiments discussed here were preformed. This facility was designed to allow basic studies of supersonic reacting flows using conventional and non-intrusive diagnostic techniques. It consists of a natural gas fueled vitiator, transition flange, interchangeable facility nozzle (Mach-1.8 and 2.2 currently available), modular isolator, modular combustor, instrument section and calorimeter. The rig is mounted to a thrust stand capable of measuring thrust of up to 2000 lbf. The test rig is provided with continuous flow of up to 30 lbm/sec at 750 psia at a temperature of up to 1660 °R, and exhausts into a 3.5 psia continuous flow exhauster system. The facility can simulate flight conditions from Mach 3.5 to Mach 5 at flight dynamic pressures of up to 2000 psf. The 36" long modular combustor has a 1.5" x 4" inlet cross-section with a constant 2.36° or 4° divergence angle. There are removable side wall inserts each 24" long to provide for optical access and modular body and cowl side inserts to allow for interchangeable fuel injection/flame holding concepts. The nozzle, isolator, and combustor are instrumented with static pressure taps, thermocouples, and heat flux gauges. Optical access is available at the exit plane, through the combustor side wall inserts, and at three separate locations in the isolator. The test facility is capable of providing heated gaseous or heated liquid hydrocarbon fuels to the test rig. The instrumentation suite includes a 256-channel electronic pressure scanning system, a 64-channel thermocouple scanning system, and 128 channels of discrete analog inputs (64 additional thermocouple channels and the remainder for other instrumentation). The other direct-connect supersonic combustion facility (Room 22) offers similar features but at a larger scale (2.5X). This facility has been described in detail elsewhere.[1, 2]

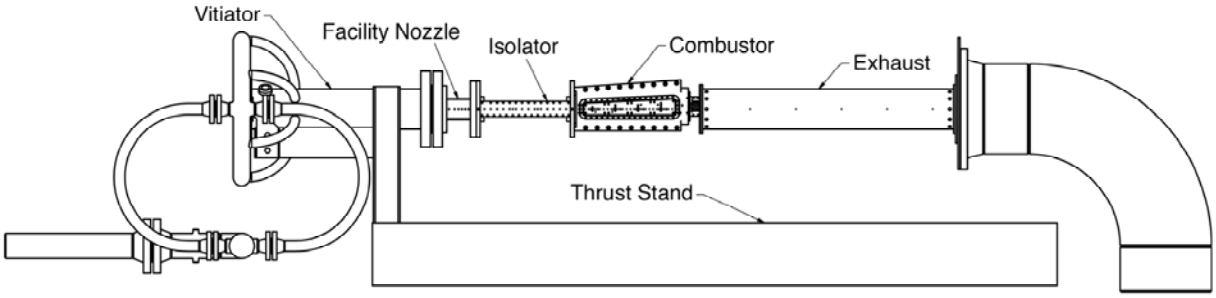

Figure 1. Schematic of Research Cell 18 combustion facility at WPAFB.

The experiments were carried out using one of the three isolators designed and fabricated for the facility. These isolators have been characterized experimentally and computationally.[3, 4] The isolator used in this study, labeled I-1 in references [3] and [4], has a rectangular cross-sectional area with a height of 3.8 cm (1.5 in), a width of 10.2 cm (4.0 in), and a length of 65.4 cm (25.75 in). Pressure taps and thermocouple ports are positioned along the centerline of each wall of the rectangular isolator. The interior surface of the isolator is coated with a layer of 0.5-mm (0.02") thick thermal barrier coating (TBC) to prolong the testing duration and to protect the metal wall from excessive heating by the vitiated hot air. The coating surface has a roughness of 13.2-15.5 μm ($520\text{-}610 \times 10^{-6}$ in).

The sidewalls of the I-1 isolator were modified for this study to allow for optical access in three locations. Figure 2 shows the modified isolator side panels with three 1 in × 3.4 in window ports. These ports are designed to hold 1.7 cm (0.68 in) in thick quartz windows or steel inserts. The quartz windows are wedged at 5º on the outer surface to prevent etaloning. The steel inserts are the same geometry as the windows, are coated with the same TBC coating as the other interior surfaces of the isolator, and have pressure taps and temperature ports at the same intervals. No difference in isolator performance has been noted between the using the quartz windows or the TBC coated steel inserts despite the differences in surface roughness between the quartz and the TBC.

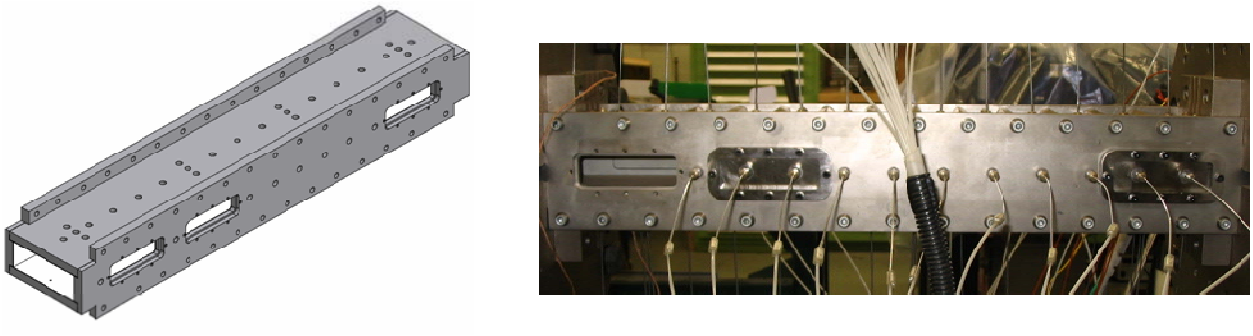

Figure 2. 25.75 inch isolator with optical access, left is a design layout and right is photograph of the isolator installed in the facility.

The isolator is connected at the exit of a nominal Mach-1.8 facility nozzle with corresponding cross-sectional configuration to produce supersonic flow. A natural-gas-fueled vitiator upstream of the facility nozzle heats the air to the desired temperature. Simulation of selected flight conditions is carried out by varying the temperature and pressure using the vitiator and by varying the isolator exit pressure using the back pressure valve. In earlier studies, the combustor module downstream of the isolator was replaced by a probe housing assembly with a throttle valve installed further downstream. A probe assembly consisting of four pitot tubes and two thermocouples was integrated into the probe housing and was used to measure pitot pressure and stagnation temperature at the exit of the extension piece. These data were used to characterize the isolator performance for a range of simulated flight conditions.[3, 4] The flight conditions calibrated to date include flight Mach numbers from 3.5 to 5.0 and dynamic pressures from 500 to 2000 psf. Unvitiated (cold) flows have also been studied.

III. Experiment

TDLAS employs single mode diode lasers that are temperature stabilized and current tuned over atomic and molecular absorption features. Molecular oxygen can be detected and quantified by tuning over selected transitions of the $b^1\Sigma_g^+$ - $X^3\Sigma_g^-$ (atmospheric) system at 760 nm.[5] Scanning multiple transitions enables the oxygen concentration to be determined as well as the static temperature. By directing one laser beam upstream and another downstream, the oxygen transitions will be shifted in frequency due to the Doppler effect, thereby enabling the flow velocity to be determined from the separation of the two absorption features in frequency space. These data provide the flow density and velocity and provide a direct measurement of the mass flux. The optical arrangement employed in Research Cell 18 is shown below in Figure 3.

One of the most noted concerns with TDLAS is the fact that it is a line-of-sight (LOS) optical technique. Figure 4 below shows the temperature, total density, and velocity profile across the Research Cell 18 rectangular 2-D isolator of 10.2 cm (4.0 in) width, 3.8 cm (1.5 in) height at a Mach 5, Q=500 psf flight condition. The distance scale corresponds to the distance traversed by the beams crossing the isolator at mid-height at $\theta = 45^o$ as defined in Figure 3. This case is fairly representative of 2-D isolator profiles and shows that both the density and velocity are low close to the isolator sidewalls. The resulting mass averaged velocity, which is what TDLAS measures, is very close to the average velocity of the core flow, i.e. the effects of averaging over the low velocity boundary layer region are minimized. Furthermore, since the velocity profiles are relatively constant in the isolator, the density variations have little effect on the average. This level of accuracy is certainly sufficient for many applications such as real time fuel injection systems and variable geometry inlets. If more precise information is required, the measured line-of-sight averaged profile can be corrected in post processing with the aid of calculated CFD profiles such as those shown in Figure 4.

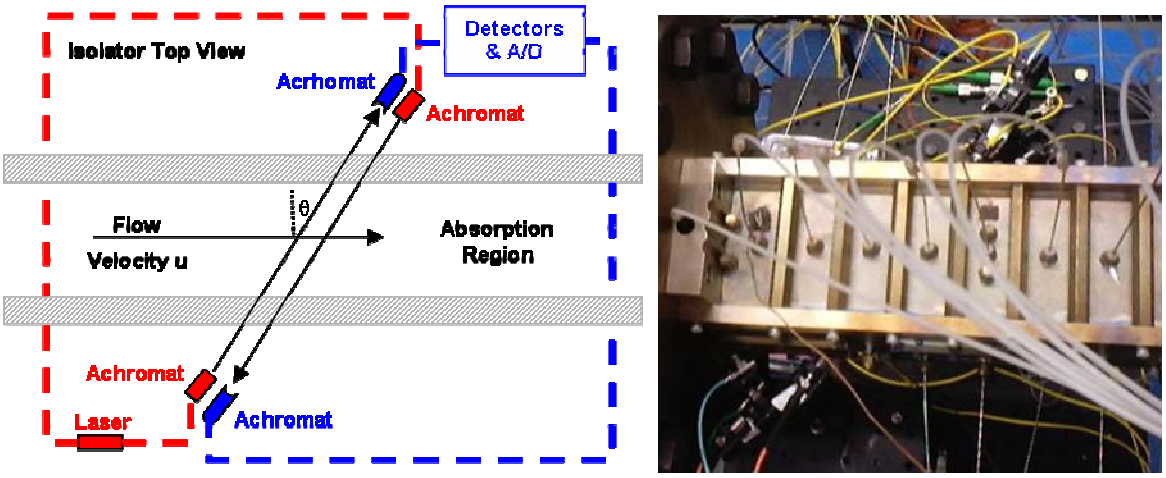

Figure 3. Laser beam geometry (top view) for velocity and concentration measurement (left) schematic (right) photograph of experiment at WPAFB.

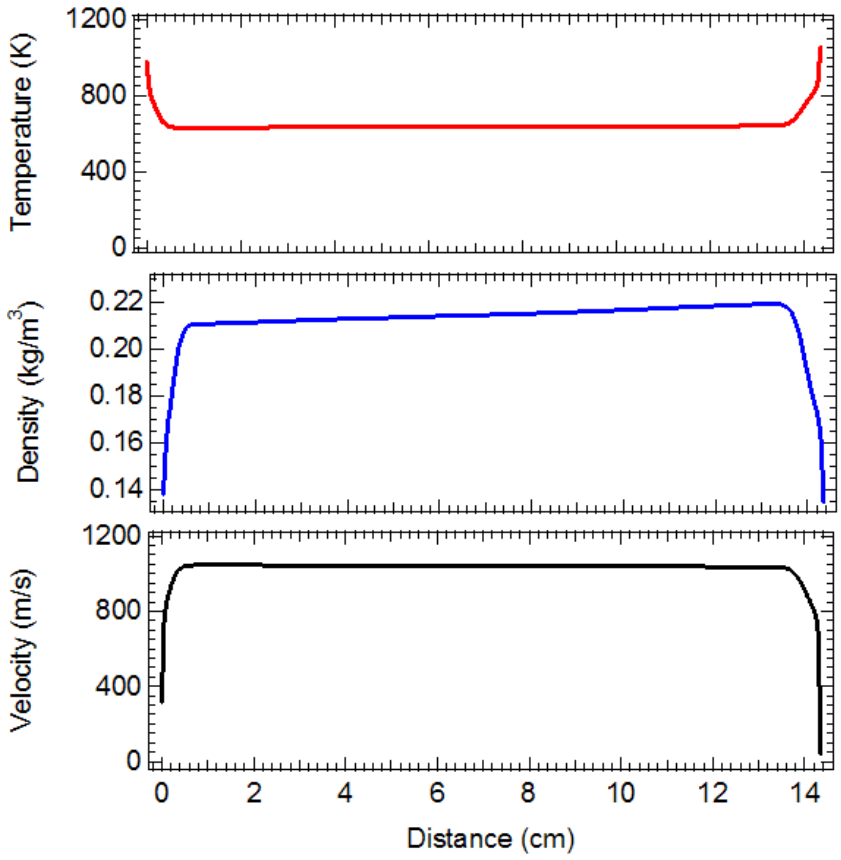

Figure 4. CFD-Calculated static temperature, total density, and velocity profiles for the 2-D isolator at WPAFB operating at a Mach 5.0, *Q*=500 psf flight condition. The distance scale corresponds to the distance traversed by the beams crossing the 10.16 cm width isolator at θ = 45º.

IV. Diode Laser System Description

The major components of the ground-test optical system include a) an Adlink Computer to process and record detected signal levels, b) the seven lasers at wavelengths of 760 nm, 1343 nm, 1348 nm, 1391 nm, 1397 nm, 1559 nm, and 1627 nm, c) an ILX driver (LDC-3916) to control the current and temperature of the lasers, d) a Stanford Research System synthesized function generator (DS335) to provide the current modulation signal to the ILX driver, e) multiplexers (Zolo Technologies and Newport Corporation) to combine and extract individual laser wavelengths to and from fiber optic cables, and f) a series of ultra low noise detector banks (Zolo Technologies) to record signal levels of the system.

The Adlink computer is a NuPRO-842 series with a full-size PICMG 1.0 Pentium 4-based single board computer with Intel 845GV chipset. The CPU module supports a front side bus of 533MHz and a maximum CPU clock of 3.06 GHz and a 32-bit/33MHz PCI/ISA bus with 2GB of high performance DDR host SDRAM support. The six near IR lasers are standard telecom fiber coupled distributed feedback (DFB) diode lasers in 14-pin butterfly packages (NEL America, Inc.). The oxygen laser included in the system is an Avalon Photonics vertical cavity surface emitting laser (VCSEL) laser (AVAP-760SM). All lasers are single mode with spectral bandwidths <2 MHz. The function generator controls the frequency and wavelength scanning range of the lasers by supplying a triangle waveform at a frequency ranging from 10-40 kHz.

The Zolo Single Mode (ZSM) multiplexer is used to combine the various near IR laser wavelengths to a single output fiber. A fraction of this multiplexed output is then sent directly back to a Zolo Multi-Mode (ZMM) de-multiplexer and is recorded on individual detector boards to create reference signals for each absorption signal channel. Indium gallium arsenide (InGaAs) detectors are used for the near-IR wavelengths and silicon (Si) detectors are used for the 760 nm channels. The remaining multiplexed signal is delivered through the absorption region and sent to another ZMM for absorption signal processing. The multiplexed laser wavelengths from the reference and signal ZMMs are then sent to individual photodiode detector boards. Note that non-telecom wavelengths (760nm) are not processed through ZSM or ZMM multiplexers at this time but are separated using a coarse wavelength division de-multiplexer (CWDM).

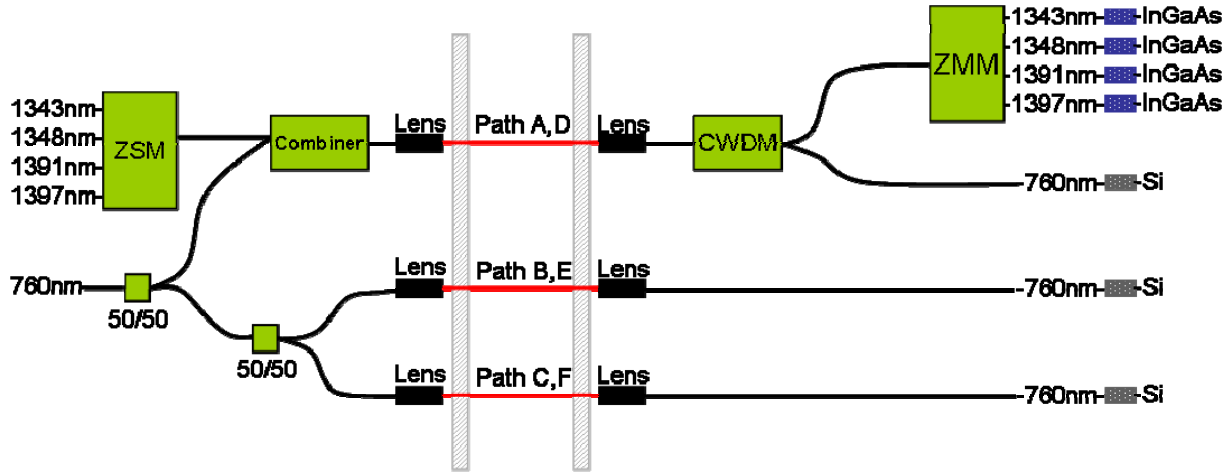

Figure 5. Schematic of optical arrangement. Paths A-C cross the test section at the exit of the isolator, Paths D-F cross the test section 3.8 inches downstream of the isolator entrance.

Figure 5 shows a schematic of the optical layout used to probe the isolator of the Research Cell 18 combustion facility at WPAFB. The general layout sketched in Figure 5 shows how three optical paths were used simultaneously. For the first series of tests, the three optical paths were constructed to have the optical characteristics of Paths A, B, and C listed in Table 1 and passed through optical windows located at the end of the isolator. Later tests used optics with characteristics of Paths D, E and F listed in Table 1, and the paths were aligned through the isolator at a distance of approximately 3.8 in downstream of the isolator entrance. Single mode sending fibers are used to deliver lasers through the absorption region; SMF28 fiber carries multiplexed near IR radiation and SM750 fiber is used to deliver the 760 nm radiation. The SMF28 and SM750 fibers are combined using a Newport combiner (F-CPL-B12355) just before being delivered to an achromat collimated sending lens for Paths A and D. In order to compare different optical geometries under nearly identical conditions two additional paths were added. The two additional beam paths at 760 nm were created using two sequential 50/50 fiber splitters. The

collimated laser radiation for each path is transmitted across the supersonic air path and received by a collimated achromat lens assembly. The beam diameter is approximately 1 mm for all beam paths. The lenses are mounted in a collar that fits into a 3-axis Thorlabs fiber optic positioning mount. The transmitted radiation is delivered to a multimode receiving fiber. The multimode signal is then delivered to the control rack where it is de-multiplexed (if required), and each channel is measured with an ultra low noise detector. The signals are then ratioed to their respective reference channels to produce transmission spectra. For the experiments discussed here, the 1559 nm and 1627 nm InGaAs detectors were replaced with Si detectors to support the simultaneous detection of the two additional 760 nm (oxygen) beam paths in the optimization studies discussed below.

Table 1. Optical characteristics of each path through the absorption region shown in Figure 5.

Path	Lambda (nm)	Send FL (mm)	Receive FL (mm)	Core (μm)	NA	Location	External Air Path (cm)	Internal Flow Path (cm)
A	1343, 1348, 1391, 1397, 760	6.2	4.5	50	0.21	Isolator Exit	28	10
B	760	12	2.0	50	0.21	Isolator Exit	28	10
C	760	6.2	2.0	100	0.29	Isolator Exit	28	10
D	1343, 1348, 1391, 1397, 760	4.5	6.2	50	0.21	3.8 in Downstream of Isolator Entrance	7.6	15
E	760	4.5	6.2	100	0.29	3.8 in Downstream of Isolator Entrance	11.6	12
F	760	6.2	11	200	0.22	3.8 in Downstream of Isolator Entrance	11.6	12

V. Optical System Design: Noise Reduction in Unvitiated (Cold) Flow

The first series of experiments were designed to assess expected signal-to-noise ratio under supersonic Mach-1.8 flow conditions. Three optical paths, Paths A, B and C were aligned though the 1 inch thick quartz sidewall windows of the combustor at the exit of the isolator section and had a total optical path length of 43 cm (28 cm for external lab air path, 5 cm for the quartz window path, and 10 cm for the internal supersonic flow path). The three paths (A-C) were configured as shown in Figure 5 with the optical components listed in Table 1. All paths were collimated for minimum beam divergence.

Figure 6a shows the transmitted laser power as a function of point number for Path A in the case of no flow. The transmitted laser power increases as the laser current is increased. Increasing the laser current also scans the frequency output of the laser. At point 100, the laser current is decreased and the frequency is scanned in the reverse direction. Increasing or decreasing the laser current varies the frequency output of the laser and thereby enables transmission/absorption spectra to be obtained. Therefore, each spectral feature is scanned twice in one waveform which is acquired at 10 kHz. Dividing these waveforms by reference frequency spectral scans collected simultaneously on an identical detector array yields the transmission spectra shown in Figure 6b. In the transmission spectra shown in Figure 6b, spectral features resulting from water and oxygen absorption can be clearly seen in the region of point numbers 50 and 150. For the purposes of discussion, the x-axis of the acquired spectra have not been converted from point to frequency space which is done in a later section by calibrating the laser current to frequency response with a high finesse etalon.

Figures 6c and 6d show the same spectra acquired during supersonic flow conditions. For this test, the total temperature and pressure inside the vitiator were 530º R and 50 psia, respectively. This test condition produced a flow velocity near Mach 1.8 with a static temperature and pressure of 329º R and 5 psia, respectively, in the vicinity of all beam paths. With the onset of the supersonic flow, the optical power transmitted through the duct fluctuated rapidly at 10% peak-to-peak or more. This noise can be seen clearly in the transmission spectrum shown in Figure 6d and can even be seen in the raw transmitted laser power shown in Figure 6c. Note the scan rate is 10 kHz which makes the method relatively insensitive to mechanical vibrations and other low frequency noise sources. The bandwidth of the noise seen in (c) and (d) extends to about 200 kHz and drops off rapidly above that frequency. In spite of the transmission noise, there was very little static attenuation of the optical signal. This implies that the magnitude of the gross beam steering had to be quite small. This was confirmed by measuring the position walk of

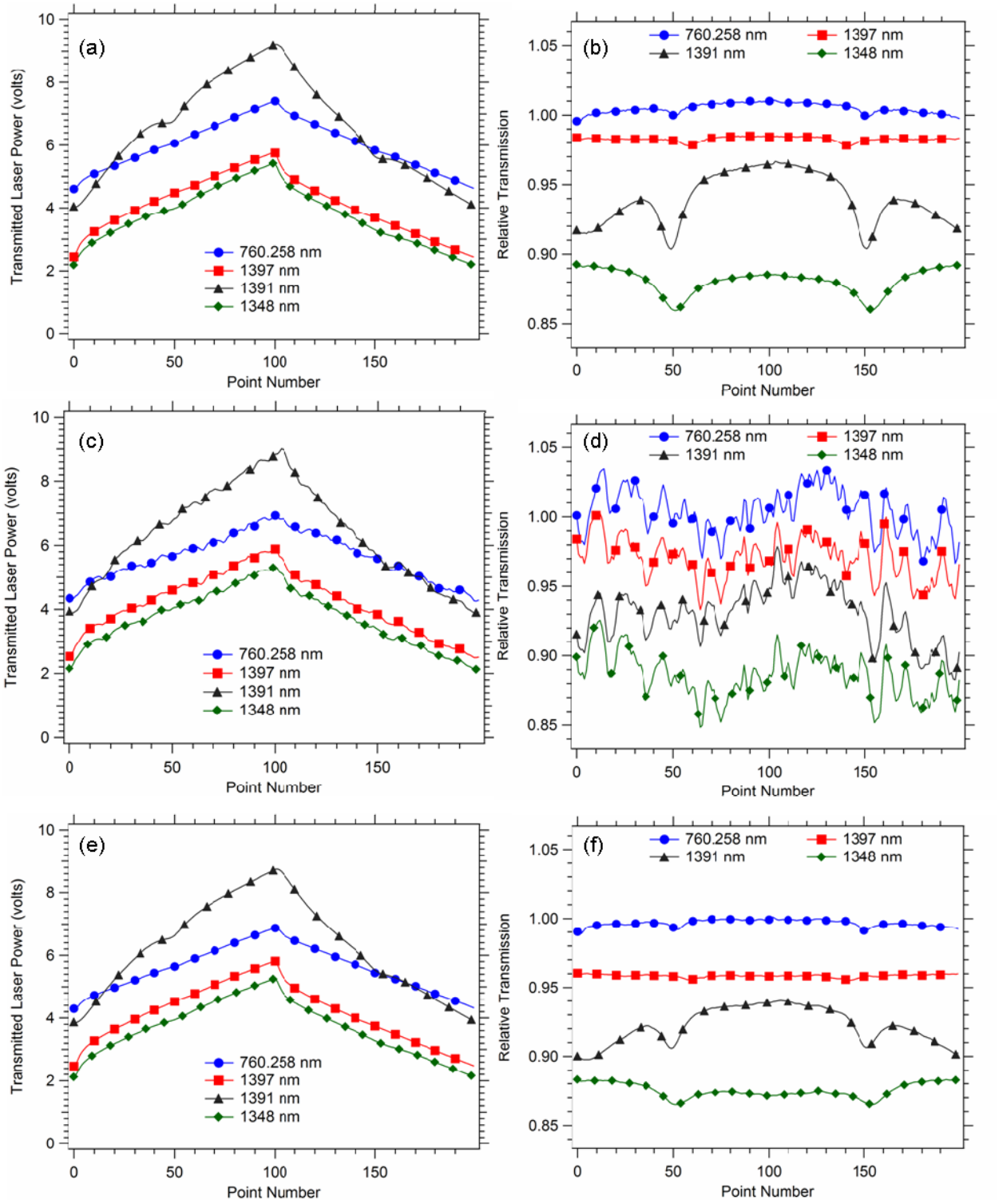

Figure 6. Transmitted laser power (a), (c), (e) and transmission spectra (b), (d), (f) for different flow conditions and averaging for Path A. (a) and (b), quiescent gas, 0.3 ms acquisition (3 averages), (c) and (d), Mach-1.8 air flow, 0.3 ms acquisition (3 averages), (e) and (f), Mach-1.8 flow, 1 s acquisition (10,000 averages).

a HeNe laser beam passing through the same region as the TDLAS beams which confirmed that the gross beam steering was 1 milliradian or less. Furthermore, there was little correlation of the transmission fluctuations for the three paths. But there was excellent correlation for the fluctuations occurring at the different wavelengths on Path A, the multiplexed path, i.e., the transmission noise was comparable and very well correlated at all wavelengths from 760 nm to 1397 nm. This transmission noise dominated over detector noise in nearly all cases. Since the transmission noise is random in nature, averaging more scans was very effective in increasing the SNR. With 1-second acquisition time (10,000 averages), high SNR spectra could be collected in the Mach-1.8 flow and shown in Figure 6 (e) and (f). During most of the testing, the beam paths were well upstream of any shock fronts, but by adjusting back pressure, shock fronts could be moved to the vicinity of the beams. When a shock front was moved into the beam path, the observed transmission noise only increased by a factor of two.

Comparing the noise from the three different paths establishes that Path C with 100 um core fiber was the best by nearly a factor of three. Path A was second best. The improvement realized with the 100 um core fiber results from two factors. First, the larger core does provide additional beam steering tolerance because of the bigger target and the larger numerical aperture (NA) (0.21 versus 0.29). Second, the larger core improves the collection efficiency thereby increasing the signal at the detector and reduces the detector noise contribution. Path B, which had been designed to give greater tolerance to beam steering, was the worst performer. Path B was designed to avoid total loss of signal even in cases where beam steering exceeded 10 milliradians by defocusing the beam. In this case, defocusing the beam led to reduced signal levels at the detector and very little improvement in signal-to-noise since the magnitude of the beam steering is not large. In other words, defocusing increases the detector noise contribution which is already a significant issue due to the rather feeble power provided from the 760 nm VCSEL. The use of a reference beam to improve the SNR was also explored since the noise was well correlated at the different frequencies. The result (not shown) was an improvement of the Path A noise limit by about a factor of two making it comparable to Path C. Based on these results, the noise appears to be best reduced by using larger-core fibers and by choosing send and receive optical focal lengths to minimize the sensitivity of the optical system to noise resulting from fast but small (sub-milliradian) beam steering. However, in the case of significant static beam steering, the use of a reference beam may also be warranted.

The primary results in terms of absorption spectra for Path A are shown in Figure 7a, i.e., the transmission spectra of Figure 6b were converted to absorption spectra and the baseline was corrected (flattened) using a second order polynomial. In Figure 7a, the laser is scanned at 10 kHz , and data acquired for 0.3 msec (3 averages) are plotted. In order to improve upon this result, the optimum send-and-receive optical setup must minimize noise due to fast but small (sub-milliradian) beam steering. This improvement was attempted using Paths D-F. An excellent discussion of optical design in beam steering environments is presented by Kranendonk and Sanders in reference [6]. In this three-path system through the isolator, the three paths were configured at angles from 29 to 48 degrees relative to the isolator window normal with total path lengths (including windows) ranging from 26 to 27 cm. Details of the optical paths are provided in Table 1.

Figure 7b shows the data obtained using optical Path D. Note that paths D-F cross the isolator section at the most upstream window (see Figure 4) at a distance of approximately 3.8 inches downstream of the isolator entrance. Again the laser is scanned at 10 kHz and 3 scans are averaged to produce the final results. Obviously the SNR is much better for the Path D data. Note the factor of 10 reduction in the y-axis scaling for Figure 7b compared to 7a. The improvement is primarily due to the fact that the focal lengths for the transmitting and receiving optics have been optimized for the low amplitude but fast beam steering previously discussed.[6] In addition, the total path length was also shortened from ~ 43 cm (Path A-C) to ~ 26 cm Path (D-F) which reduced the lever arm, and hence, the magnitude of the beam steering.

The noise for Paths D, E and F (not shown) are not noticeably different despite the fact that the paths have the 50, 100, and 200 micron receive fibers, respectively. This suggests that the alignment of the optics was much better optimized for the Path D-F data leading to much better tolerance to the beam steering. Thus the 50 micron data is as good as either of the larger core fiber data. However, given that perfect alignment is not always possible and that loss of perfect alignment may occur during flight, it makes sense to use the largest core fiber that is compatible with the system multiplexer technology.

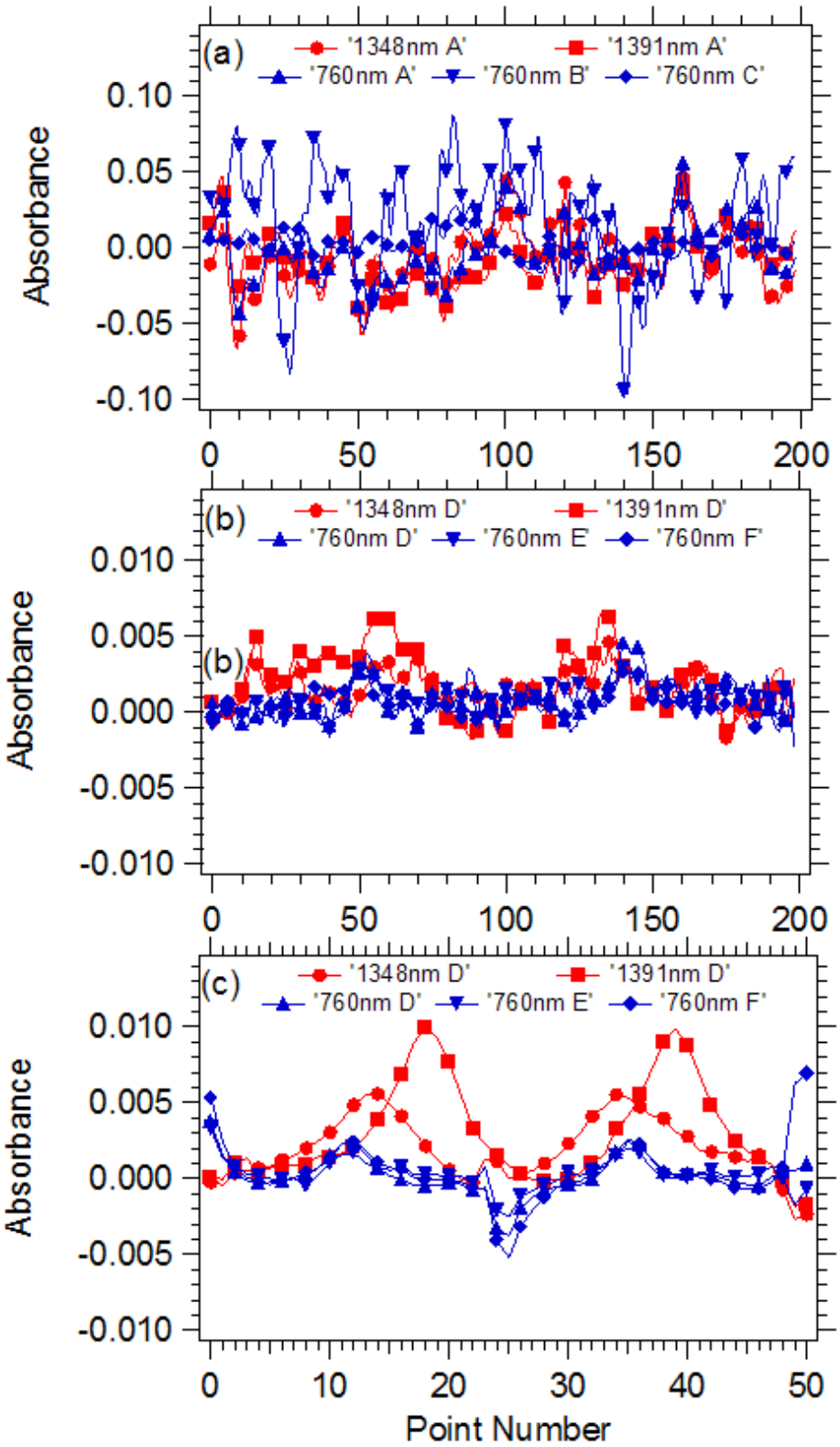

Figure 7: Absorption spectra at various wavelengths though Mach-1.8 unvitiated (cold) air flow. The laser repetitively scans the spectrum 0.3 ms of data are averaged to produce spectra. (a) Path A, 10 kHz, 0.3 ms acquisition (3 averages), (b) Path D, 10 kHz, 0.3 ms acquisition (3 averages), (c) Path D, 40 kHz, 0.3 ms acquisition (12 averages).

Figures 8a and 8b demonstrate a noticeable improvement in the optical geometry leading to less sensitivity to high frequency flow noise. An additional improvement in SNR can be gained by increasing the scan rate of the laser from 10 kHz to 40 kHz. Increasing the scan rate has a two-fold impact. First, more averages can be obtained in the same time interval which leads to a significant improvement in SNR as shown in Figure 6. Second, the frequency response of the observed flow fluctuations is significant all the way up to about 100 kHz. As the scanning frequency approaches this frequency, there is substantial improvement in SNR because the noise follows an ~1/f curve. Figure 7c shows data acquired for 0.3 msec with the laser scan rate increased to 40 kHz. In this case, 12 scans are averaged to produce the spectrum shown. The data quality is improved significantly, and this SNR is now adequate to measure Doppler shift spectra during flight. Furthermore, this spectrum can be acquired at a rate of 3000 Hz, which far exceeds the present requirements for a mass flux measurement which is in the 10 Hz range. However, the downside of faster scanning is that four times fewer points (50 vs. 200) are sampled across the waveform for a fixed data system sampling rate. This reduced number of points results in less frequency resolution, and hence, less velocity resolution. In addition, note that the "tails" at the beginning and end of the spectra shown in Figure 7c result from improper timing of the data acquisition cards which is significant at rapid scanning frequencies. With a custom DSP-based high-speed data acquisition system, it is expected that these artifacts could be greatly improved or completely removed. Furthermore, increasing the scanning frequency above 40 kHz would be advantageous but is not currently possible due to the need for a detection bandwidth out to several harmonics of the scan frequency. However, if this were technically possible, preliminary estimates indicate that an optimal scanning frequency is in the 150 kHz range.

VI. System Operation: Vitiated (Hot) Flow

The data from Paths D-F discussed above were also used to characterize the flow in the isolator in a nominal Mach 1.8 vitiated flow. The wind tunnel was operated with conditions which simulate flight Mach numbers of 3.5 and 4.0 and a dynamic pressure of 1000 psf for the research scramjet configuration. To achieve these simulated flight conditions, a compressed natural gas fueled vitiator was used to elevate the air temperature entering the Mach 1.8 facility nozzle. For the Mach 3.5 flight condition, the total temperature and total pressure inside the vitiator are 1253º R and 52.1 psia, respectively. For the Mach-4.0 flight condition, the total temperature and total pressure inside the vitiator are 1398 R and 53.5 psia, respectively. In all cases, a "make up" amount of oxygen is supplied to the vitiator so that the composition of the gas exiting the nozzle had an oxygen mole fraction of 0.21. Note that the mole fraction of nitrogen is decreased compared to air in this case to accommodate the presence of the combustion products, namely, carbon dioxide and water, formed in the vitiator. The peak oxygen absorption was about 0.2% under these simulated scramjet flight conditions at the probed location which was approximately 3.8 inches downstream of the isolator entrance. The water and oxygen concentrations for this test condition and location are 2.2×10^{17} molecules/cm^3 and 1.8×10^{18} molecules/cm^3, respectively.

Figure 8 shows the results obtained for Path D for the Mach 3.5 condition. Compared to the case of the cold flow involving unvitiated dry air, the vitiated flow has combustion products present. Hence a large increase in water absorption signals is observed resulting in absorption signal levels approximately 50 times larger than those observed for oxygen, despite the fact that there is about an order of magnitude less water in the flow path. The peak water absorption was about 10% under these conditions compared to the peak oxygen absorption signal of 0.2%, which is typical for the analysis of post-combustion products.[7] The weak absorption is a direct result of the fact that the available technology necessitates the use of the weak transitions of the $b^1\Sigma_g^+ - X^3\Sigma_g^-$ (atmospheric) system at 760 nm.[5]

As was shown in Figure 7, increasing the scan rate from 10 to 40 kHz greatly improves the signal-to-noise level due to increased averaging as evidenced by comparing the data shown in Figure 8a taken at 10 kHz to those of Figure 8b taken at 40 kHz. This transmission noise for the spectra shown in Figure 8b for Path D is about 100 times better than the original Path A results. The noise baseline has been significantly reduced and is now sufficient to attempt to make real time velocity measurement under simulated flight conditions. The data in Figure 8c substantiates this point and shows that 10 ms of data acquisition provides waveforms of sufficient SNR to process to obtain the velocity (shift of the spectral feature) and density (integral of the spectral feature) information necessary to determine the mass flux.

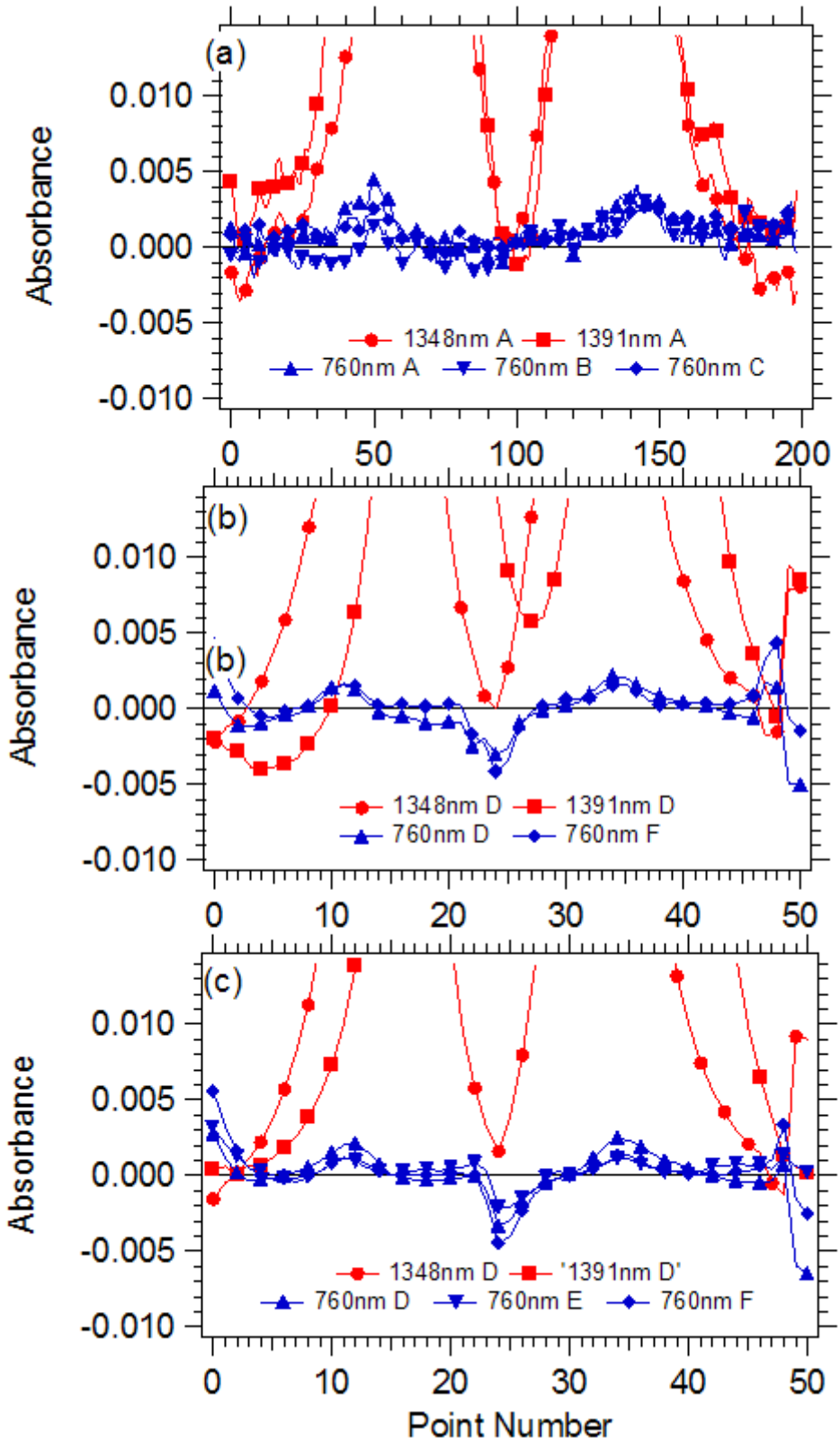

Figure 8: Absorption spectra at various wavelengths though high-speed flow. The laser repetitively scans the spectrum 0.3 ms of data are averaged to produce spectra. (a) Path A, 10 kHz, 3 scans (0.3 ms) (b) Path D, 40 kHz, 12 scans (0.3 ms) (c) Path D, 40 kHz, 400 scans (10 ms)

VII. Velocity Measurement

To perform the velocity determination, counterpropagating paths, as shown in Figure 3, were set up to obtain the Doppler shift measurement at an angle, θ, of 38.3º. For this measurement, the two paths were made as symmetric as possible, with nominally-identical fibers, optics and path lengths, and the external beam paths were purged with dry nitrogen. Light from both paths was sent through GIF50 fiber directly to detectors and both signal levels were comparable. While investigating the signal quality during test preparations, an apparent polarization-switching behavior in the VCSEL was observed. This behavior, which was also present during parts of the previous tests, led to noise in the absorption spectrum which varied dramatically with fiber position. The polarization switching occurred at about 760.255 nm, partially obscuring the absorption line at 760.258 corresponding to the $^{R}Q(13)$ transition.[5] The VCSEL was then retuned to 760.094 nm corresponding to the $^{R}Q(15)$ transition[5] in order to eliminate this behavior from the VCSEL's scanning range. The temperature in the vitiator was then increased in 100º R increments from 798º R to 1593º R in order to provide calculated flow velocities from 600 m/s to 850 m/s based on isentropic equations. Signals from both counterpropagating paths and reference signals were recorded with varied acquisition times at scan rates of 10 kHz and 40 kHz. An example of a spectrum obtained for the quiescent gas inside the isolator (no flow) is shown in Figure 9a. As can be seen the absorption features for the two scans are nearly identical indicating that the two paths are well matched in intensity and are not shifted with respect to each other in frequency.

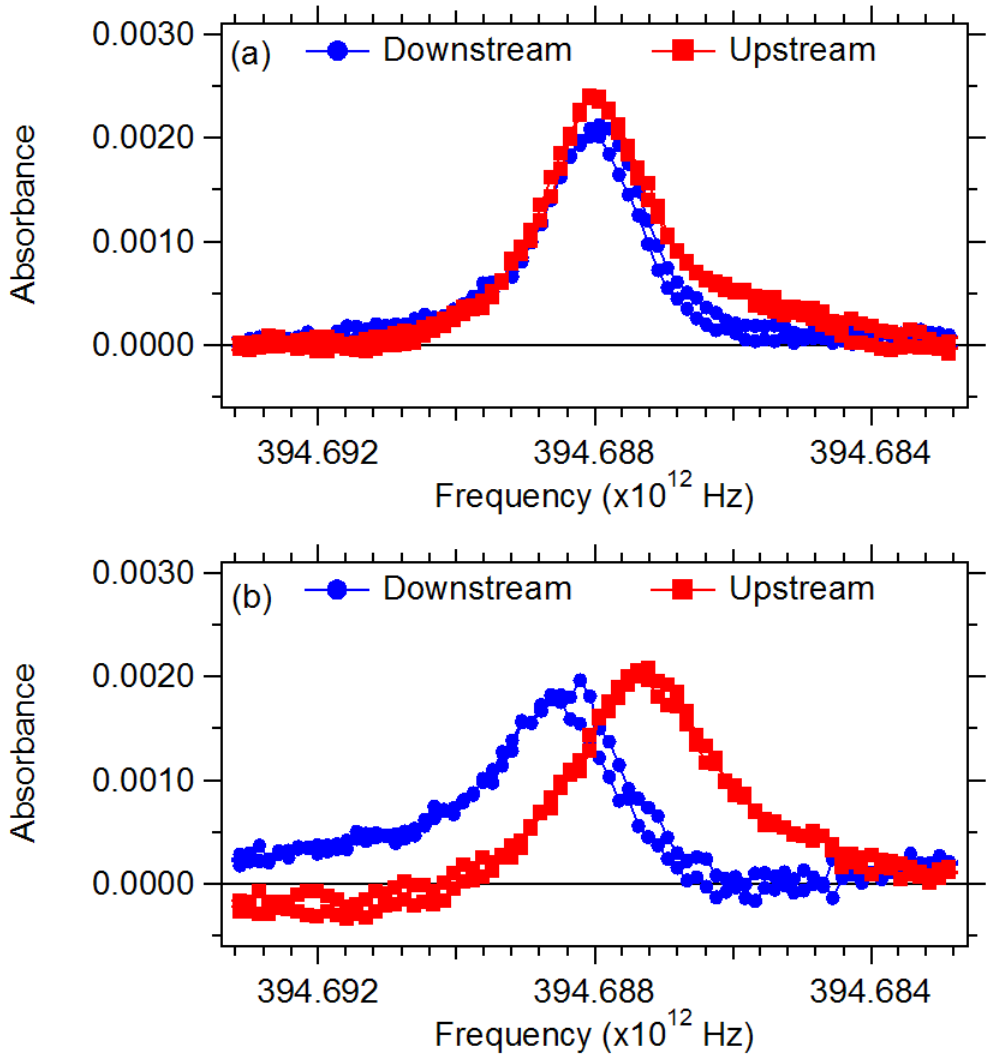

Figure 9: Absorption spectra at 760.094 nm scanned at 10 kHz with 100 ms of acquisition (1000 averages) (a) No flow (b) Mach-1.8 flow corresponding to a Mach-4.0 flight condition

Figure 9b shows the spectrum obtained with the flow on for the Mach 4.0 flight condition, Q=1000 psf corresponding to a total temperature and pressure inside the vitiator of 1397° R and 52.1 psia, respectively. The oxygen concentration for this test condition is 1.8×10^{18} molecules/cm^3. The frequency shifts of the upstream and downstream propagating beam paths are clearly seen in Figure 9b compared to Figure 9 a. The frequency shift and crossing angle can be used to deduce the mass averaged flow velocity across the isolator using the geometry shown in Figure 3 and Eq. (1) below

$$\Delta\nu = \nu_o (2\sin\theta)\frac{u}{c} \tag{1}$$

where ν_o is the line center frequency, u is the bulk flow velocity, c is the speed of light, and $\Delta\nu$ is the frequency difference between the two peaks resulting from the Doppler frequency shift from the line center frequency. These results are plotted in Figure 10 for two of the measurement cases evaluated in this study.

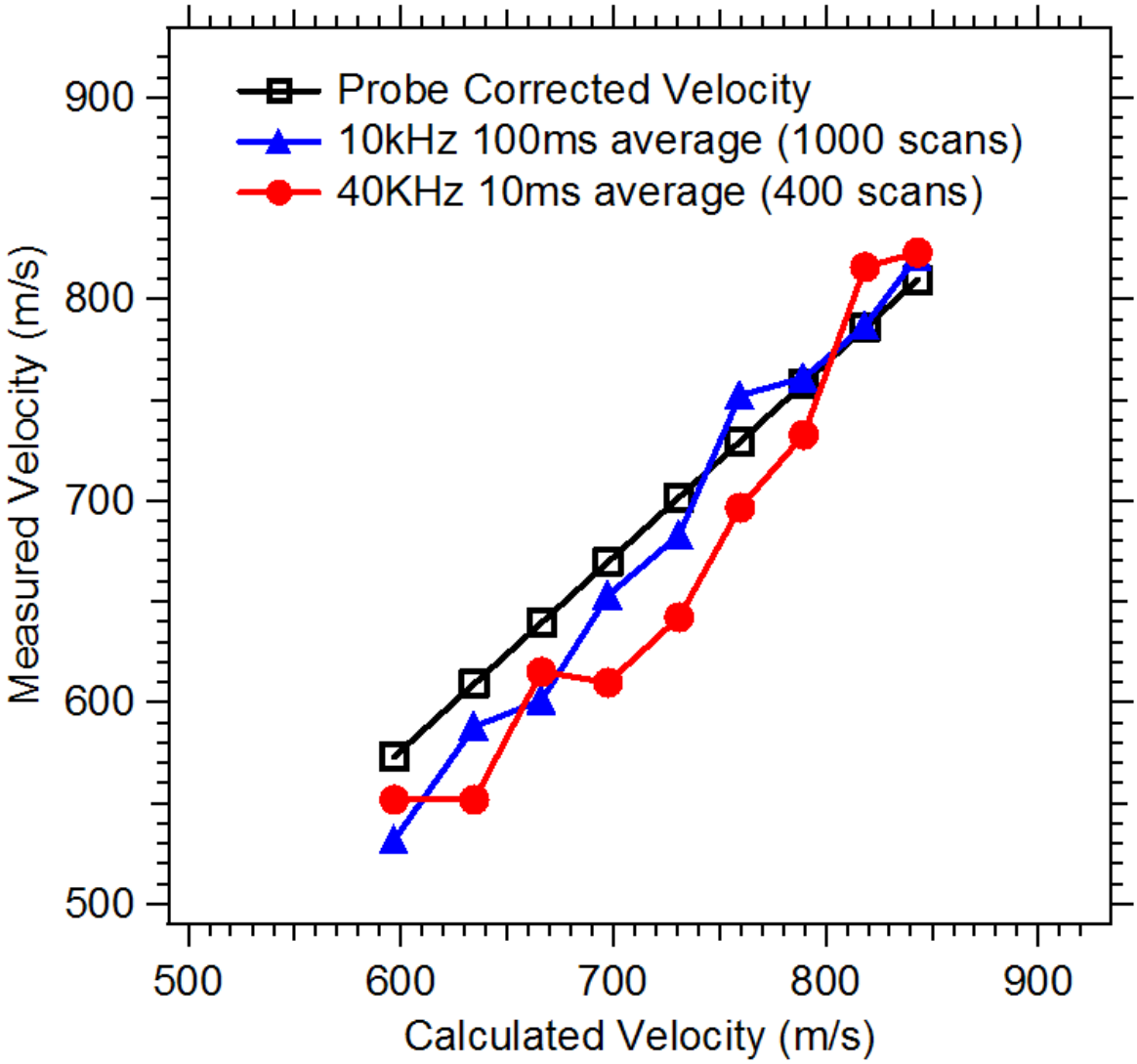

Figure 10: Pitot and thermocouple probe corrected velocity and optically measured (Doppler shift) velocity vs. calculated velocity for an ideal nozzle.

The measured velocities are plotted in Figure 10 vs. the calculated velocity for an ideal nozzle operating under fully isentropic conditions. However, this calculated velocity is too high because it does not account for the entropy rise due to wall friction. Therefore, the pitot pressure and thermocouple temperature probe measurements discussed earlier were used with the calculated values to derive the mass averaged flow velocities sampled over these test conditions. These derived values are labeled probe-corrected velocity and are plotted on the y-axis for comparison to the optical measurements. The correction applied is based on the data listed in Table 2 which contains the results of some measurements made with a pitot and thermocouple probe placed 3 inches downstream of the nozzle exit for the Mach 3.5 and Mach 4.0 test conditions. This location is close to the location of the counterpropagating 760 nm beam paths which was approximately 3.8 inches downstream of the nozzle exit. The probe was scanned in the spanwise (horizontal) direction at midheight in the isolator and in the vertical direction at the midway point in the spanwise direction. These probe scans are labeled horizontal and vertical, respectively, in Table 2. The probe measurements are recorded in Table 2 and show that the mass averaged velocity is approximately 0.96 of the calculated isentropic velocity for the horizontal probe direction and approximately 0.95 of the calculated isentropic velocity for the vertical probe direction. The vertical and horizontal probe directions yield nearly the same value for the mass averaged velocity suggesting that the velocity profile is relatively uniform across the path traversed by the laser beams. These measurements are supported by CFD calculations such as those shown in Figure 4. Therefore, it is assumed that the calculated isentropic velocity can be scaled by 0.96 since the laser beams traverse the isolator at midheight at an angle θ of 38.3º. The calculated isentropic velocities were multiplied by 0.96 and labeled Probe Corrected Velocity in Figure 10.

Table 2. Pitot and thermocouple probe measurements at three inches downstream of the isolator exit.

P_o(psia)	T_o(R)	Probing direction	Ideal nozzle exit velocity (Isentropic) (m/s) u_1	Measured maximum velocity (m/s) u_2	Measured mass-averaged velocity (m/s) u_3	u_3/u_1
52.0	1253	Horizontal	747.5	730.8	718.0	0.96
51.9	1257	Vertical	748.7	718.4	698.4	0.93
51.6	1255	Vertical	748.0	729.2	713.4	0.95
53.5	1406	Horizontal	791.8	772.3	762.4	0.96
53.5	1401	Vertical	790.5	762.9	741.6	0.94
53.1	1404	Vertical	791.3	775.9	754.6	0.95

In Figure 10, it appears that the optically measured velocity is systematically lower at the low velocity range. This effect may be due in part to applying the correction universally over the entire range when the probe calibration was only performed over the 720 m/s to 775 m/s range. Other possibilities are that the external beam paths were not effectively purged with dry nitrogen and some of the cold, quiescent oxygen in the external beam path has been averaged into our measurements. Carefully matching the beam paths and purging should minimize these effects, but the signal levels were so low for these experiments that it is difficult to completely eliminate this source of interference. Another source of error relates to the accuracy to which the crossing angle θ can be measured on the test stand. Errors of a degree can lead to measured velocity errors of a few percent. Future experiments will employ alignment masks to increase the accuracy to which the crossing angle can be determined.

Despite these issues, the data plotted in Figure 10 is very encouraging because it demonstrates that oxygen density and velocity can be measured under realistic flight conditions with data update rates approaching 100 Hz. In this initial study, the TDLAS velocity data agree to within 22 m/s and 32 m/s (1 σ) for the 10 kHz and 40 kHz data, respectively. The 10 kHz scans afford better velocity resolution at present due to increased sampling and better frequency resolution. However, the 40 kHz scans offer better SNR for shorter acquisition times. The next series of experiments will involve multiplexing the 760 nm and 1391 nm lasers so that the oxygen and water velocity measurements can be obtained simultaneously. The water absorbance signals are approximately 50 times larger in intensity which should increase the accuracy of the measurements and provide, in essence, an internal standard for the development of the oxygen sensor.

VIII. Conclusions

Tunable diode laser absorption spectroscopy was used to measure the air velocity in the isolator section of a research scramjet flowpath. Tests were conducted in the isolator section of the Research Cell 18 direct connect wind tunnel facility at WPAFB. The flow in the isolator was found to introduce a small amount of high frequency beam steering but no true attenuation due to gross beam walk. The transmission noise was almost completely eliminated by employing send-and-receive optics and fibers that were designed to capture nearly all of the laser radiation traversing the isolator experiencing 1 milliradian beam steering or less. Since the optical paths were short and well-aligned and since the beam steering was of small amplitude, all of the transmitted light could be captured with a fiber as small as 50 um. However, in the presence of static misalignments (due to heating, low-frequency vibrations, etc.), larger beam steering, or with longer paths, larger receive fiber cores are expected to improve performance and allow for operation in the noise-free plateau. Therefore the largest core size that is practical should be integrated into the receive optical assembly. A dramatic improvement in SNR for a constant data acquisition time was observed when the scan frequency was increased from 10 kHz to 40 kHz. This increased performance was due increased signal averaging and a lower sensitivity to the high frequency beam steering noise which has a 1/f character. However, the mismatch in the frequency response of the signal and reference detectors produced large tails at the turning points in the 40 kHz data. Therefore, scanning at the higher frequencies introduces electronic and software challenges, but definitely improves SNR if fast flow noise dominates as in this case.

The improved optical and electronic TDLAS system detected water and oxygen at concentrations of 2.2×10^{17} cm^{-3} and 1.8×10^{18} cm^{-3}, respectively, in the isolator of the Research Cell 18 supersonic combustion facility operated at simulated flight Mach numbers of 3.5 and 4.0 and a dynamic pressure of 1000 psf. The velocity was determined at these conditions and above and below by varying the vitiator temperature in 100º R increments from 798º R to 1593º R in order to provide calculated flow velocities from 600 m/s to 850 m/s based on isentropic equations. The TDLAS data agree to with 22 m/s and 32 m/s (1 σ) for the 10 kHz and 40 kHz data, respectively. The 10 kHz scans afford better velocity resolution at present due to increased sampling and better frequency resolution. The 40 kHz scans offer better SNR for shorter acquisition times. These results are very encouraging because they demonstrate that oxygen density and velocity can be measured under realistic flight conditions with data update rates approaching 100 Hz.

Acknowledgments

This work was sponsored by the AFRL/Propulsion Directorate under contract numbers F33615-03-D-2326 and FA8650-05-C-2533 and by Air Force Office of Scientific Research (Dr. Michael Berman, Program Manager). Assistance from the air facility group of the Air Force Research Laboratory is acknowledged. Also, the authors thank Paul Kennedy, Matt Streby, Steve Enneking, William Terry, and Kevin Kirkendall for their great assistance in rig operation, data acquisition, and hardware design and setup. The authors thank Dr. John Tam, Dr. Dean Eklund, Dr. Jay Jeffries and Professor R. K. Hanson for helpful discussions.

References

[1] M. Gruber, Donbar, J., Jackson, K., Mathur, T., Baurle, R., Eklund, D., and Smith, C., "Newly Developed Direct-Connect High-Enthalpy Supersonic Combustion Research Facility," *Journal of Propulsion and Power,* vol. 17, pp. 1296-1304, 2001.

[2] T. Mathur, Gruber, M., Jackson, K., Donbar, J., Donaldson, W., Jackson, T., and Billig, F., "Supersonic Combustion Experiments with a Cavity-Based Fuel Injector," *Journal of Propulsion and Power,* vol. 17, pp. 1305-1312, 2001.

[3] K.-C. Lin, C.-J. Tam, K. R. Jackson, D. R. Eklund, and T. A. Jackson, "Characterization of Shock Train Structures inside Constant-Area Isolators of Model Scramjet Combustors," *44th AIAA Aerospace Sciences Meeting and Exhibit,* vol. AIAA 2006-0816, 9-12 January, 2006.

[4] K.-C. Lin, C.-J. Tam, D. R. Eklund, K. R. Jackson, and T. A. Jackson, "Effects of Temperature and Heat Transfer on Shock Train Structures inside Constant-Area Isolators," *44th AIAA Aerospace Sciences Meeting and Exhibit,* vol. AIAA 2006-0817, 9-12 January, 2006.

[5] S.-L. Cheah, Y.-P. Lee, and J. F. Ogilvie, "Wavenumbers, strengths, widths and shifts with pressure of lines in four bands of gaseous $^{16}O_2$ in the systems $a^1\Delta_g$-$X^3\Sigma_g^-$ and $b^1\Sigma_g^+$-$X^3\Sigma_g^-$," *J. Quant. Spectrosc. Radiat. Transf.,* vol. 64, pp. 467-482, 2000.

[6] L. A. Kranendonk and S. T. Sanders, "Optical design in beam steering environments with emphasis on laser transmission measurements," *Appl. Opt.,* vol. 44, pp. 6762-6772, 2005.

[7] J. T. C. Liu, Rieker, G. B., Jeffries, J. B., Hanson, R. K., Gruber, M. R., Carter, C. D., and Mathur, T., "Near-Infrared Diode Laser Absorption Diagnostic for Temperature and Water Vapor in a Scramjet Combustor," *Applied Optics,* vol. 44, pp. 6701-6711, 2005.